


Two-dimensional rare-earth halide based single-phase triferroicSrishti Bhardwaj¹ and T. Maitra^{1*}*Department of Physics, Indian Institute of Technology Roorkee, Roorkee 247667, Uttarakhand, India* (Received 4 November 2022; revised 6 June 2023; accepted 1 August 2023; published 22 August 2023)

Two-dimensional multiferroic materials are highly sought after due to their huge potential for applications in nanoelectronic and spintronic devices. Here, we predict, based on first-principle calculations, a single-phase *triferroic* where three ferroic orders—ferromagnetism, ferroelectricity, and ferroelasticity—coexist simultaneously in the hole doped GdCl₂ monolayer (a ferromagnetic semiconductor). This is achieved by substituting 1/3rd of the Gd²⁺ ions with Eu²⁺ in the hexagonal structure of the GdCl₂ monolayer. The resulting metallic state undergoes a bond-centered charge ordering driving a distortion in the hexagonal structure, making it semiconducting again and *ferroelastic*. Further, the lattice distortion accompanied by a breaking of the lattice centrosymmetry renders a noncentrosymmetric charge distribution, which makes the monolayer *ferroelectric*, at the same time. The two ferroic orders, ferroelectricity and ferroelasticity, present in the Eu-substituted GdCl₂ monolayer are found to be strongly coupled, making it a promising candidate for device applications. The Eu-substituted monolayer remains a ferromagnetic semiconductor with a large *4f* magnetic moment just like the parent monolayer and possesses an even higher (out-of-plane) magnetic anisotropy energy than its pristine counterpart as desired for two-dimensional magnets to have high transition temperature.

DOI: [10.1103/PhysRevB.108.L081116](https://doi.org/10.1103/PhysRevB.108.L081116)

Multiferroic materials, i.e., the materials possessing two or more ferroic orders simultaneously, present a potential avenue for multistate nonvolatile memory storage and various other multifunctional device applications via the cross coupling between different ferroic orders [1,2]. However, this coexistence of more than one ferroic order is not very common, especially in two-dimensional (2D) materials. It is due to the Mermin-Wagner theorem [3], which does not allow the spontaneous magnetic ordering in 2D materials and, also, large depolarization field in ultrathin films, which destroys the vertical polarization [4,5]. Also, the mechanisms of ferroelectricity (FE) and ferromagnetism (FM) are mutually exclusive, thus making the coexistence of FE and FM and hence the realization of magnetoelectric multiferroics rare [6]. Despite these difficulties, quite a few two-dimensional multiferroic materials showcasing two ferroic orders simultaneously have been predicted, some of which are also experimentally realized recently [7,8]. However, only a very small number of 2D materials possessing all the three orders [FE, FM, and ferroelastic (FA)], i.e., *triferroics*, have been reported so far [9–11]. These materials are very promising for multifunctional device purposes and hold possibilities for novel physical phenomena. Also, in order for these materials to be directly integrated into the conventional semiconductor circuits, it is preferable for them to be semiconducting in nature.

Recently, a series of 2D FM semiconducting monolayers based on rare-earth halides [GdX₂ (X = Cl, Br, I)] have been predicted [12,13]. These monolayers have large magnetization: 8μ_B per formula unit (f.u.) owing to strong intraion Gd_{4f}-Gd_{5d} orbital interaction and large magnetic anisotropy

energies due to large spin-orbit coupling. Their Curie temperatures are predicted to be quite high (more than 220 K) due to strong superexchange interaction between Gd-5*d* orbitals via halogen *p* orbitals [12,13]. The band gap values of monolayer GdCl₂, GdBr₂, and GdI₂ calculated within the PBE+*U* method are found to be 0.89, 0.82, and 0.60 eV, respectively [13]. Recently, another rare-earth based monolayer GdI₃ with honeycomb lattice is identified as an antiferromagnet from first principles calculations which when doped with electrons via intercalation of metal atoms (Li and Mg) displays Fermi surface nesting [14]. This makes the monolayer undergo Peierls transition which, assisted by the electron-phonon coupling, generates ferroelasticity in the monolayer. Simultaneously, the ground state magnetic configuration of the monolayer changes from AFM to FM, making it a FM-FA multiferroic.

In order to explore the possibilities for multiferroicity caused by similar phenomenon, we choose the GdCl₂ monolayer, with the largest band gap among the GdX₂ (X = Cl, Br, I) monolayers, for hole doping. Although, we do not observe a similar Peierls dimerization as seen in GdI₃ [14], we observe a bond-centered charge ordering within the unit cell which generates a spontaneous strain in the lattice. Owing to the threefold rotational symmetry of the parent lattice, the charge ordering can take place along three different orientations, which makes the strain switchable rendering the monolayer ferroelastic. Also, the deformation of lattice leads to a breaking of centrosymmetry resulting in a finite spontaneous polarization. We further show that the ground state magnetic configuration of the monolayer remains ferromagnetic. Thus the hole-doped GdCl₂ monolayer is found to be ferroelectric, ferromagnetic, and ferroelastic simultaneously, making it a single phase *triferroic*. Moreover, the

*tulika.maitra@ph.iitr.ac.in

ferroelectricity and ferroelasticity of the monolayer are found to be strongly coupled.

The first-principle calculations are performed using density functional theory (DFT) as implemented in the Vienna *ab initio* Simulation Package (VASP) [15]. In order to deal with the core electrons, we have used the projector augmented wave (PAW) method [16], whereas the kinetic energy cutoff for the plane waves is set at 500 eV. For the exchange correlation functional, we have used the Perdew-Burke-Ernzerhof (PBE) parametrization [17] of the generalized-gradient approximation. The standard pseudopotentials were used for all the atoms with the electronic configurations $5s^25p^64f^75d^16s^2$ for Gd, $5s^25p^64f^75d^06s^2$ for Eu, and $3s^23p^5$ for Cl atoms. The Hubbard correlation is taken into account using the rotationally invariant GGA (PBE)+ U method [18] with $U_{\text{eff}} = U - J = 4.0$ eV (here U is Coulomb correlation and J is Hund's exchange) for both Gd and Eu $4f$ orbitals, the value having been adopted from previous work [13]. Treatment of f electrons using PBE+ U is possible as f subshell is half filled. We have also studied the effect of variation of U_{eff} on our results for several U_{eff} values (see Table S1 and Fig. S1 in the Supplemental Material [19]) and observed that our results presented below remain robust against the variation of U . The structures are relaxed until the Hellmann-Feynman forces are reduced to 0.01 eV/Å and the energy convergence criteria is set at 10^{-6} eV. A Γ centered $11 \times 11 \times 1$ Monkhorst-Pack grid was chosen for electronic structural optimization. Vacuum of size 18.5 Å was inserted between two monolayers to avoid interlayer interactions. In order to check if the vacuum added is sufficient, we have calculated and plotted the planar average of the electrostatic potential between successive monolayers along the c direction (see Fig. S2 of the Supplemental Material [19]). We can see that the vacuum size of 18.5 Å considered in our calculation is sufficient. The phonon dispersion calculations were performed using the density functional perturbation theory (DFPT) as implemented in VASP and the PHONOPY package with a $3 \times 3 \times 1$ supercell [20,21]. To check thermal stability, *ab initio* molecular dynamics (AIMD) calculations were performed where we used the *NVT* ensemble at 300 K using a Nosé Hoover thermostat. The simulation was performed for 15 ps with a time step of 3 fs [22].

GdCl₂ monolayer has hexagonal crystal structure with space group $p\bar{6}m2$. Each monolayer consists of three atomic layers: one Gd atom layer sandwiched by two Cl atom layers as shown in Fig. 1. Each Gd ion is coordinated by 6 Cl atoms forming a trigonal prismatic cage (see Fig. 1). The calculated optimized lattice constants of the GdCl₂ monolayer are $a = b = 3.78$ Å, which are similar to the previously reported values [13]. Also, it is found to be a FM semiconductor with a magnetic moment of around $8\mu_B$ per Gd atom and a band gap of 0.88 eV, in close agreement with the reported values [13]. We substituted 1/3rd of all Gd sites by Eu in the GdCl₂ monolayer, i.e., we replaced Gd atoms present at the center of each Gd hexatomic ring with Eu atoms [Fig. 2(a)]. The formation energy for this substitution is found to be -6.22 eV/f.u. under Cl-rich condition and -0.16 eV/f.u. under Gd-rich condition as calculated using the formula

$$E_f = E(\text{Gd}_2\text{EuCl}_6) - E(\text{Gd}_3\text{Cl}_6) + \mu_{\text{Gd}} - \mu_{\text{Eu}},$$

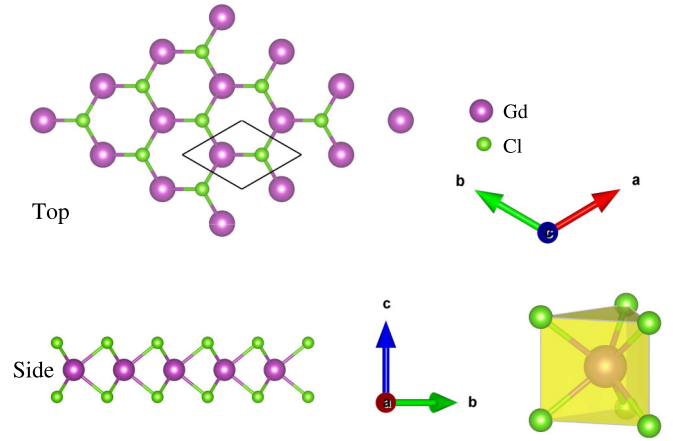


FIG. 1. Top (upper panel) and side (lower panel) views of the crystal structure of the GdCl₂ monolayer where solid black rhombus in the top view represents the primitive cell. GdCl₆ trigonal prismatic cage is shown in yellow on the right side of the lower panel.

where $E(\text{Gd}_2\text{EuCl}_6)$ and $E(\text{Gd}_3\text{Cl}_6)$ represent the energy of Eu-substituted and pristine $\sqrt{3} \times \sqrt{3} \times 1$ supercell of the GdCl₂ monolayer, respectively, whereas μ_{Gd} and μ_{Eu} represent the chemical potentials of Gd and Eu. We take the energy per atom of the bulk Eu (orthorhombic) as μ_{Eu} . For the value of μ_{Gd} , we considered both the Gd-rich and Cl-rich conditions: under the Gd-rich condition, μ_{Gd} is taken as the energy per Gd atom in the bulk hexagonal crystal structure, whereas under the Cl-rich condition, μ_{Gd} is the difference in energy of a GdCl₂ ML unit cell and that of a Cl₂ molecule. The negative value of the formation energy under both conditions (Gd-rich and Cl-rich) confirms the feasibility of the substitution process. The oxidation state of Eu atoms doped in GdCl₂ ML is +2, the same as that of Gd, and hence their electronic configuration is $4f^7d^0$. The Eu d orbitals are energetically close to the Gd d orbitals causing a finite overlap between them.

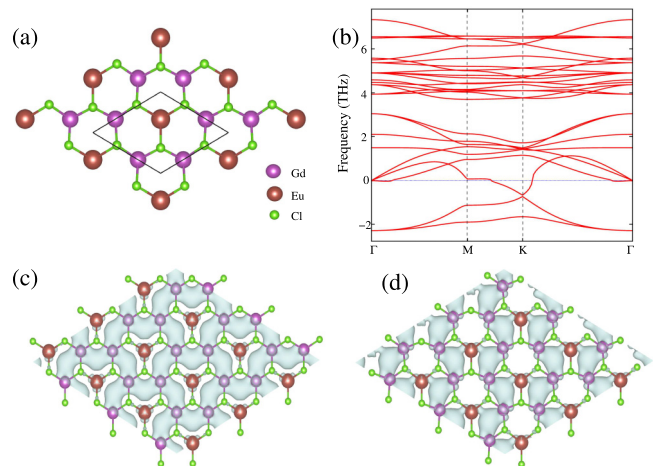


FIG. 2. (a) Top view of the high-symmetry hexagonal 1/3 Eu-substituted GdCl₂ monolayer. (b) Phonon dispersion for the hexagonal symmetric structure of the Eu-substituted monolayer showing soft phonon modes. (c) Centrosymmetric and (d) noncentrosymmetric charge density distributions before and after relaxation of the substituted structure, respectively.

Thus the given Eu substitution amounts to a 1/3rd hole doping in the valence band of the pristine GdCl₂ monolayer, making the doped monolayer metallic. However, the resulting metallic hexagonal structure of the doped monolayer is unstable, as indicated by the soft phonon modes present in its phonon spectrum [see Fig. 2(b)], towards a bond-centered charge ordered state where the charge density localizes on four out of six Gd-Gd bonds on the hexagonal ring of Gd ions surrounding each Eu [Fig. 2(d)] accompanied by corresponding lattice distortions. The atomic displacements corresponding to the soft phonon modes are shown in Fig. S3. For comparison we show in Fig. 2(c) the uniform charge density distribution on all the six Gd-Gd bonds in the unstable structure. The corresponding lattice distortions are obtained upon performing a full relaxation of the unit cell (removing all the symmetry constraints). The four Gd-Gd bonds with finite charge density residing on them are found to be shortened, while the other two are elongated. Also, the Eu atoms initially placed at the center of the Gd hexatomic rings shift away from the center making the structure noncentrosymmetric. The final relaxed structure thus becomes polar with space group *Amm*2. The top and side views of the relaxed structure are shown in Fig. 3(a) with various Gd-Gd/Gd-Eu bond lengths (d1–d4) marked. The comparison between the nearest neighbor Gd-Gd and Gd-Eu bond lengths and the lattice parameters in the initial hexagonal and the relaxed deformed structure is given in Table I. The phonon spectrum for the relaxed structure no longer shows the soft phonons indicating its dynamical stability [Fig. 3(b)]. Further, to check the thermal stability, we performed the *ab initio* molecular dynamics (AIMD) simulation at a temperature of 300 K for 15 ps with a time step of 3 fs. There are only small fluctuations in energy and the structure remains almost intact after 15 ps [Fig. 3(c)].

In order to understand the bond centered charge ordering and associated lattice distortions observed in our system, we looked at various possible scenarios. Though we observed Fermi surface nesting in the high symmetry metallic phase, we do not observe any unit cell doubling expected from Peierls dimerization as observed in GdI₃ [14]. So we believe the charge ordered state that we observe in our system is unlikely to be associated with Peierls-like transition. This charge ordered state could be similar to the “Zener polaron order” state observed in doped manganites [23,24], which involves both Zener double exchange and a polaroniclike distortion between the Gd and Eu sites with finite charge density between them. As Zener double exchange is known to drive a ferromagnetic order between localized spins and also as all the Gd and Eu atoms share more than one such “Zener polaron bonds,” the spins at all the atoms in the crystal are expected to align in a FM pattern. However, further calculations and experiments are needed to establish the mechanism.

To probe the magnetic ground state of Eu-substituted GdCl₂ ML, we studied four different AFM configurations along with the FM one [Fig. 3(d)]. The preferred magnetic ordering is found to be FM with AFM1, AFM2, AFM3, and AFM4 magnetic configurations found to be 575.0 meV, 208.9 meV, 563.5 meV, and 378.9 meV per supercell [shown in Fig. 3(d)] higher in energy, respectively. The value of magnetization per formula unit (Gd₂EuCl₆) is found to be 21.76μ_B, which is in close agreement with the formal mag-

netic moment of 8μ_B on Gd with electronic configuration 4f⁷d¹ and 7μ_B on Eu with electronic configuration 4f⁷d⁰, in valence state +2. In Figs. 3(e) and 3(f) we present the band structure and density of states respectively for the FM state. As evident from these figures the low symmetry doped monolayer is a semiconductor with an indirect band gap of about 0.40 eV. The bands above and below the Fermi level (FL) mainly comprise spin up Gd *d* orbitals with only a small contribution from spin up Eu *d* orbitals. The Cl 2*p* orbitals mainly lie far below the FL with a little overlap of Gd and Eu *d* orbitals. Also, the localized 4*f* orbitals lie far below the FL. Thus Eu-substituted GdCl₂ ML is a half semiconductor with only spin up states closest to the FL. In order to determine the preferred direction for spin alignment, we performed spin-orbit coupling calculation which is quite important in our case as we are dealing with heavy rare-earth ions. The preferred spin orientation is found to be out of plane of the monolayer. The magnetic anisotropy energy (MAE) defined as the energy difference between the in-plane and out-of-plane spin orientations, i.e., Δ*E* = *E*_{*c*} − *E*_{*ab*}, is found to be about 790 μeV/f.u., which is higher than that of the pristine GdCl₂ monolayer [13] and hence can play a big role in stabilizing the magnetic ordering in the 2D limit. The band structure does not change much after including SOC and the band gap also remains almost unchanged.

In order to get an estimate of the value of *T*_{*c*} for the doped monolayer, we calculate the nearest neighbor magnetic exchange interaction parameters. In the deformed structure of the monolayer, we have four different kinds of nearest neighbor pairs: short and long distance Gd-Gd pairs, with distances denoted by *d*₁ and *d*₂, respectively, and short and long distance Gd-Eu pairs, with distances denoted by *d*₃ and *d*₄, respectively [see Fig. 3(a) and Table I]. Correspondingly, there are four kinds of NN exchange parameters denoted by *J*₁, *J*₂, *J*₃, and *J*₄. In order to calculate these parameters, we use the energy mapping scheme [13] using the spin Hamiltonian

$$H = -J \sum_{\langle i,j \rangle} S_i \cdot S_j - A \sum_i (S_i^z)^2,$$

where *J* is the nearest neighbor exchange parameter, *S*_{*i*} and *S*_{*j*} are spin operators, *S*_{*i*}^{*z*} is the *z* component of the spin operator, and *A* is the single ion anisotropy energy parameter. We use five different magnetic configurations as illustrated in Fig. 3(d). In accordance with the relative spin alignment of the nearest neighboring atoms, the magnetic energy expressions for these configurations per magnetic unit cell (supercell) shown in Fig. 3(d) are given as

$$E_1 = E_0 - 8J_1|S_a|^2 - 4J_2|S_a|^2 - 16J_3S_a \cdot S_b - 8J_4S_a \cdot S_b, \quad (1)$$

$$E_2 = E_0 + 8J_1|S_a|^2 + 4J_2|S_a|^2, \quad (2)$$

$$E_3 = E_0 - 8J_1|S_a|^2 + 4J_2|S_a|^2, \quad (3)$$

$$E_4 = E_0 + 8J_1|S_a|^2 - 4J_2|S_a|^2 - 8J_4S_a \cdot S_b, \quad (4)$$

$$E_5 = E_0 - 8J_1|S_a|^2 - 4J_2|S_a|^2 + 16J_3S_a \cdot S_b + 8J_4S_a \cdot S_b, \quad (5)$$

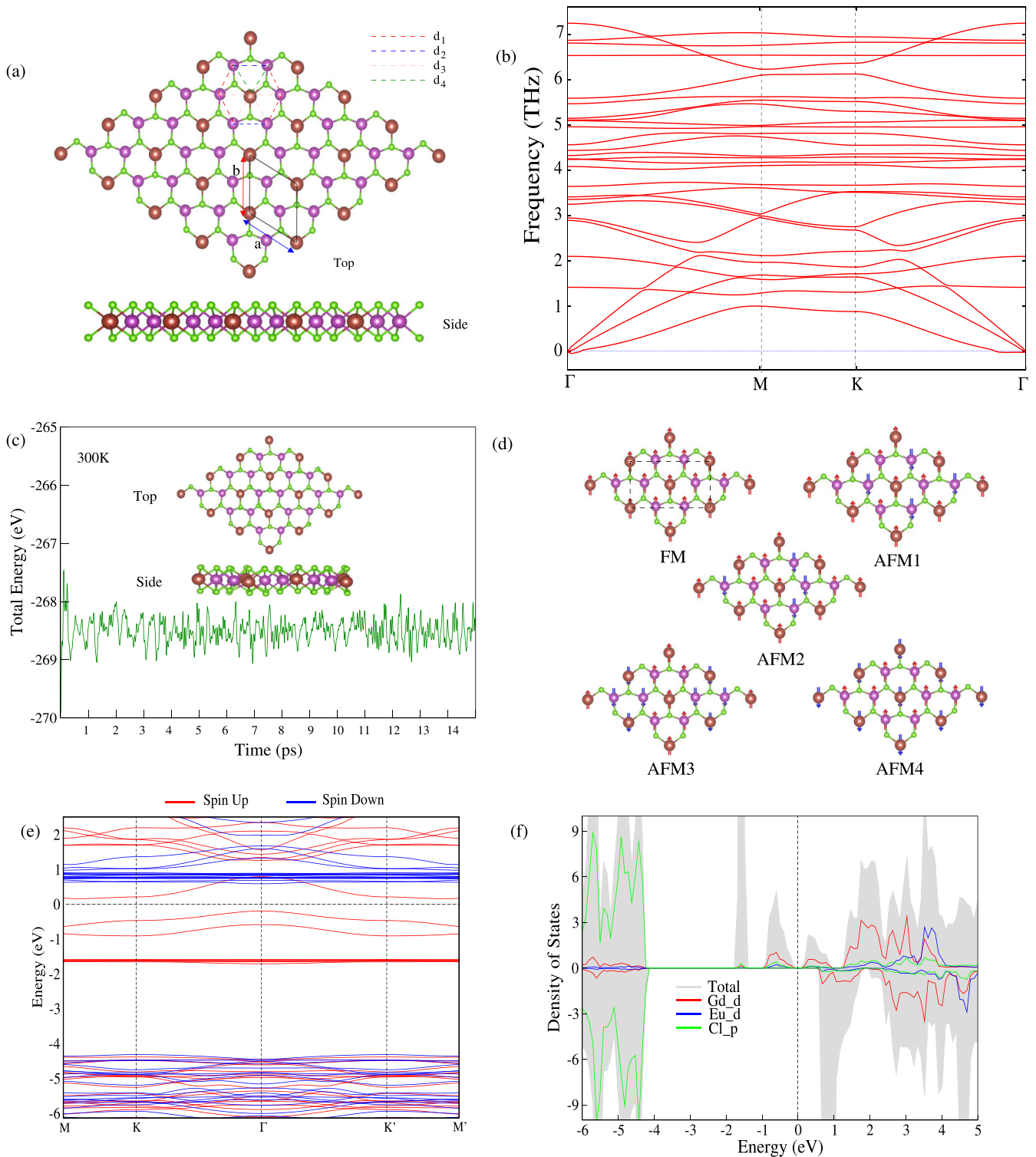


FIG. 3. (a) Top and side views of the Eu-substituted GdCl₂ monolayer after relaxation. Gd, Eu and Cl are represented by violet, brown and green spheres respectively. Red (blue) lines represent short (long) NN Gd-Gd bonds and brown (green) lines represent short (long) NN Gd-Eu bonds. (b) Phonon dispersion spectrum for the relaxed structure. (c) The fluctuation of total energy and snapshots (top and side view) of monolayer structure after 15 ps from AIMD simulation. (d) Various possible magnetic configurations for the doped monolayer. Red and blue arrows represent spin up and spin down, respectively. Black rectangle represents the unit cell used for magnetic energy calculations. (e) Spin resolved band structure and (f) total and orbital-projected partial density of states (PDOS) of the deformed doped monolayer.

TABLE I. Nearest neighboring Gd-Gd and Gd-Eu pair distances and the lattice parameter comparison between the high-symmetry ($p\bar{6}m2$) and the relaxed deformed ($Amm2$) structure of the Gd_2EuCl_6 monolayer.

Structure	d_1 (Å)	d_2 (Å)	d_3 (Å)	d_4 (Å)	a (Å)	b (Å)
Hexagonal	3.93	3.93	3.93	3.93	6.80	6.80
Deformed	3.78	4.30	3.82	4.23	6.85	6.79

where E_0 represents the sum of energy per magnetic unit cell without magnetic coupling and the magnetocrystalline anisotropy energy with spins aligned along the out-of-plane, i.e., z direction. S_a and S_b represent the spins of Gd and Eu atoms, respectively, determined by the number of unpaired electrons in valence state +2. The values of exchange parameters calculated within GGA+ U +SO using these expressions are $J_1 = 1.41$ meV, $J_2 = 0.151$ meV, $J_3 = 0.76$ meV, and $J_4 = -0.064$ meV. Thus the exchange parameters corresponding to shorter Gd-Gd and Gd-Eu bonds are significantly larger than the ones corresponding to longer bonds and ferromagnetic interaction is the most dominant one. We also observed from our GGA+ U +SO calculations that any noncollinear (canted) spin arrangement is not stable which, we believe, is because of the presence of bond-centered charge ordering (BCO) in the material where a single d electron is shared between the neighboring Gd ions. In pristine $GdCl_2$ monolayer the ferromagnetic transition temperature is predicted from Monte Carlo calculations to be $T_c = 224$ K by Liu *et al.* [13]. The values of exchange parameters and the magnetic anisotropy of the doped monolayer are higher than those of the pristine $GdCl_2$ monolayer. Thus we expect a comparable critical temperature (T_c) for the ferromagnetic phase transition.

As a result of the bond-centered charge ordering associated lattice distortion, the threefold rotational symmetry of the initial hexagonal structure is broken. The deformed structure has an increased lattice constant along a direction (6.85 Å) and a shrunk lattice constant along b direction (6.79 Å) [Fig. 3(a)], i.e., a is around 1% larger than b . Now, as the parent high-symmetry structure is hexagonal and has threefold rotational symmetry, this deformation of the lattice can occur along three different orientations [Fig. 4(a)] all of which are equally probable. Thus the Eu-substituted $GdCl_2$ monolayer can relax into three equivalent lattice configurations oriented at 120° with respect to each other. As a result, Eu-substituted $GdCl_2$ ML manifests ferroelasticity where one can switch between three equivalent lattice configurations by changing the strain direction via external mechanical stress. This switching between different configurations in the presence of external forces also makes the material stable against mechanical damage.

In order to investigate the energetics of the structural transition from one ferroelastic state to another, we performed a solid-state nudged elastic band (SS-NEB) calculation. The minimum energy pathway (MEP) for transition from one lattice configuration to another rotated at 120° is shown in Fig. 5. The transition barrier height is 120 meV/f.u., which is more than that of 2D FE-FA multiferroic MX monolayers ($M = Sn, Ge; X = S, Se$) [25], but less than that of the $GaTeCl$ monolayer [26]. Such an energy barrier indicates that the

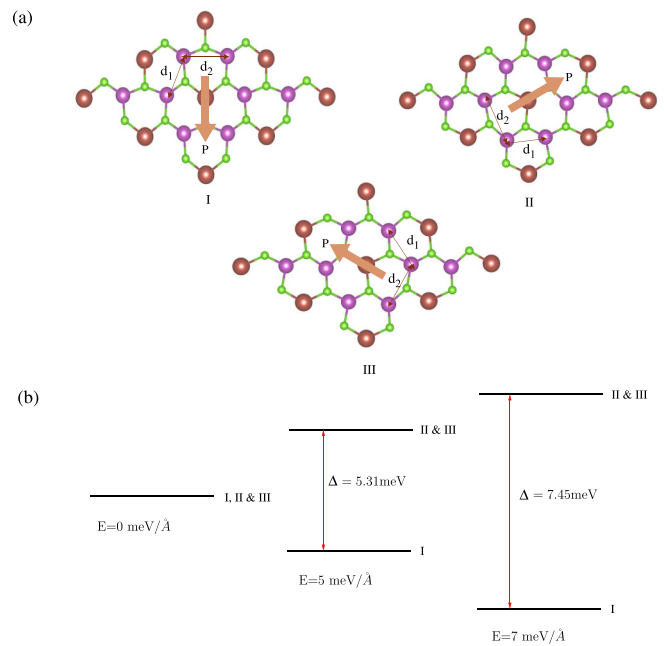


FIG. 4. (a) Different possible lattice configurations of the Eu-substituted monolayer and corresponding spontaneous polarization directions. (b) Energies of different lattice configurations under external electric field applied along the polarization direction of lattice configuration I.

ferroelastic phases of the Eu-substituted monolayer are robust at room temperature but still can be made to transit from one to the other by application of a moderate amount of external force. From our DFT calculations we found that a tensile strain of 10% along the direction of one of the shortened Gd-Gd bonds [d_1 in Fig. 4(a)] and a compressive strain of 8% perpendicular to it are required to overcome the transition

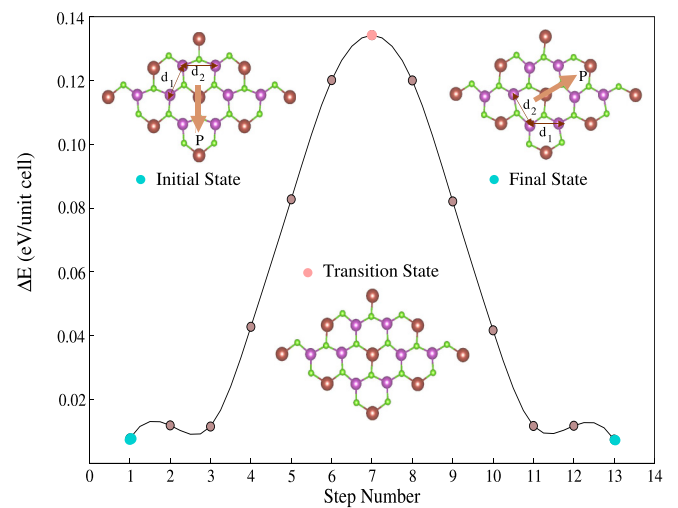


FIG. 5. Minimum energy pathway for transition from one ferroelastic (ferroelectric) phase to another as obtained using the solid state nudged elastic band (SS-NEB) method. In the inset are the initial, final, and the highest energy state acquired by the monolayer during the structural transition.

barrier and cause a phase transition from one state to another shown in Fig. 4(a).

Interestingly, since the deformed structure also involves an off-center shifting of Eu atoms leading to a noncentrosymmetric charge density distribution, we expect to observe a net spontaneous polarization. We used the modern theory of polarization using the Berry phase approach as implemented in VASP [27,28] to calculate the spontaneous polarization. To correct for the polarization quanta in the calculated polarization value due to the periodic nature of the lattice, the standard procedure is to find the polarization values for all the structures along a distortion path from the centrosymmetric (nonpolar) state to the noncentrosymmetric (polar) state [29,30]. However, in our case the centrosymmetric state and the intermediate states close to it along the distortion path (Fig. 5) are found to be metallic in nature, which makes it impossible to calculate their polarization values using the Berry phase approach. In order to eliminate the possibility of any polarization quanta involved, we followed the procedure as discussed in the last section of the Supplemental Material [19]. Thus the estimated spontaneous polarization value (after polarization quanta correction) from our calculations comes out to be ~ 36 pC/m, along the direction of Eu shifting [Fig. 4(a)]. The magnitude of polarization is comparable to that of ML $\text{Bi}_2\text{O}_2\text{S}$ (12 pC/m) [31] and $(\text{CrBr}_3)_2\text{Li}$ (92 pC/m) [32]. Since there are three possible directions for Eu off-center shifting due to the threefold rotational symmetry of the initial hexagonal lattice, one can have, correspondingly, three different polarization directions which point at an angle of 120° with respect to each other as shown in Fig. 4(a). However, since, in our system, the intermediate states along the distortion path from one FE state to another have metallic behavior, an external electric field cannot be used to switch the polarization direction unless an alternative distortion path is found where the intermediate states are insulating.

On the other hand, as the direction of spontaneous polarization is decided by the direction of charge ordering and associated lattice deformation, the polarization switching can be carried out by switching between lattice configurations with different charge ordering directions (different strain directions) using external mechanical stress, making the Eu-substituted GdCl_2 monolayer ferroelectric along with being ferroelastic and ferromagnetic. Note that our system may not fall under the category of conventional ferroelectrics where an electric field is used for switching the ferroelectric polarization; however, in our case the switching can be done via an external mechanical stress due to the strong coupling between the polarization direction and the direction of strain. A similar situation (mechanical controllability of polarization) has been previously reported in literature, for example, in GaTeCl monolayer, bismuth oxychalcogenides, etc. [26,31]. Particularly, in the case of the GaTeCl monolayer, the barrier height for polarization reversal under electric field is found to be too high (754.1 meV) and it was therefore suggested

that the ferroelectric switching can rather be done in two steps of 90° rotational transitions using external tensile stress. Thus the Eu-substituted GdCl_2 ML can be termed as a single-phase triferroic in which ferroelectricity and ferroelasticity are strongly coupled. Further, it can be shown that, on applying an external electric field, the lattice configuration with polarization direction along the direction of electric field becomes energetically favorable. For this purpose, we applied an in-plane external homogeneous electric field along the polarization directions in the lattice configurations I, II, and III using the perturbation expression after discretization (PEAD) [33,34] approach as implemented in VASP. Note that we have not relaxed the structure under external electric field as also has been done previously for another system [35]. We observe that, when the electric field is applied along the polarization direction of lattice configuration I, the energy of lattice configuration I decreases while that of the configurations II and III increase [Fig. 4(b)]. The same can be shown for the external electric field along the polarization directions of other configurations too.

In summary, we predict based on a detailed theoretical investigation that the Eu-substituted GdCl_2 monolayer would be a promising candidate material for the realization of a two-dimensional single phase triferroic where ferromagnetic, ferroelectric, and ferroelastic orders coexist. The doped monolayer is found to be thermodynamically stable from our phonon and AIMD calculations. The estimation of magnetoanisotropy energy and exchange parameters indicate that the ferromagnetic state can have a comparable transition temperature to that predicted for the parent compound GdCl_2 monolayer (~ 224 K). The hole doped GdCl_2 monolayer undergoes a bond centered charge ordering accompanied by lattice distortions, which opens a gap at the Fermi surface making the system semiconducting as well as ferroelastic. In addition, we observe shifting of Eu ions from centrosymmetric positions giving rise to ferroelectricity in the system. We have also shown through our calculations that there exists a strong coupling between ferroelectricity and ferroelasticity where one can switch among three possible orientations via external mechanical stress. Thus the Eu-substituted GdCl_2 monolayer looks to be a very versatile material for device applications.

T.M. acknowledges discussions with P. K. Choubey. S.B. acknowledges the Council of Scientific and Industrial Research (CSIR), India for research fellowship support. T.M. acknowledges the Science and Engineering Research Board (SERB), India for funding support through MATRICS research grant (No. MTR/2020/000419). T.M. and S.B. acknowledge the National Supercomputing Mission (NSM) for providing computing resources of “PARAM Ganga” at the Indian Institute of Technology Roorkee, which is implemented by C-DAC and supported by the Ministry of Electronics and Information Technology (MeitY) and Department of Science and Technology (DST), Government of India.

[1] W. Eerenstein, N. D. Mathur, and J. F. Scott, *Nature (London)* **442**, 759 (2006).

[2] K. F. Wang, J. M. Liu, and Z. F. Ren, *Adv. Phys.* **58**, 321 (2009).

[3] N. D. Mermin and H. Wagner, *Phys. Rev. Lett.* **17**, 1133 (1966).

- [4] J. Junquera and P. Ghosez, *Nature (London)* **422**, 506 (2003).
- [5] D. D. Fong, G. B. Stephenson, S. K. Streiffer, J. A. Eastman, O. Auciello, P. H. Fuoss, and C. Thompson, *Science* **304**, 1650 (2004).
- [6] N. A. Spaldin, S.-W. Cheong, and R. Ramesh, *Phys. Today* **63**(10), 38 (2010).
- [7] X. Tang and L. Kou, *J. Phys. Chem. Lett.* **10**, 6634 (2019).
- [8] M. An and S. Dong, *APL Mater.* **8**, 110704 (2020).
- [9] L. Yang and M. Wu, *Nanotechnology* **29**, 215703 (2018).
- [10] S. Shen, X. Xu, B. Huang, L. Kou, Y. Dai, and Y. Ma, *Phys. Rev. B* **103**, 144101 (2021).
- [11] L. Yang, Y. Gao, M. Wu, and P. Jena, *Phys. Rev. B* **105**, 094101 (2022).
- [12] B. Wang, X. Zhang, Y. Zhang, S. Yuan, Y. Guo, S. Dong, and J. Wang, *Mater. Horiz.* **7**, 1623 (2020).
- [13] W. Liu, J. Tong, L. Deng, B. Yang, G. Xie, G. Qin, F. Tian, and X. Zhang, *Mater. Today Phys.* **21**, 100514 (2021).
- [14] H. You, Y. Zhang, J. Chen, N. Ding, M. An, L. Miao, and S. Dong, *Phys. Rev. B* **103**, L161408 (2021).
- [15] G. Kresse and J. Hafner, *Phys. Rev. B* **47**, 558 (1993).
- [16] P. E. Blöchl, *Phys. Rev. B* **50**, 17953 (1994).
- [17] J. P. Perdew, K. Burke, and M. Ernzerhof, *Phys. Rev. Lett.* **77**, 3865 (1996).
- [18] A. I. Liechtenstein, V. I. Anisimov, and J. Zaanen, *Phys. Rev. B* **52**, R5467 (1995).
- [19] See Supplemental Material at <http://link.aps.org/supplemental/10.1103/PhysRevB.108.L081116> for the details of performed calculations and results.
- [20] X. Gonze and C. Lee, *Phys. Rev. B* **55**, 10355 (1997).
- [21] A. Togo and I. Tanaka, *Scr. Mater.* **108**, 1 (2015).
- [22] G. J. Martyna, M. L. Klein, and M. Tuckerman, *J. Chem. Phys.* **97**, 2635 (1992).
- [23] A. Daoud-Aladine, J. Rodriguez-Carvajal, L. Pinsard-Gaudart, M. T. Fernandez-Diaz, and A. Revcolevschi, *Phys. Rev. Lett.* **89**, 097205 (2002).
- [24] J. S. Zhou and J. B. Goodenough, *Phys. Rev. B* **62**, 3834 (2000).
- [25] H. Wang and X. Qian, *2D Mater.* **4**, 015042 (2017).
- [26] S.-H. Zhang and B.-G. Liu, *Nanoscale* **10**, 5990 (2018).
- [27] R. Resta, *Ferroelectrics* **136**, 51 (1992).
- [28] R. D. King-Smith and D. Vanderbilt, *Phys. Rev. B* **47**, 1651 (1993).
- [29] J. B. Neaton, C. Ederer, U. V. Waghmare, N. A. Spaldin, and K. M. Rabe, *Phys. Rev. B* **71**, 014113 (2005).
- [30] N. A. Spaldin, *J. Solid State Chem.* **195**, 2 (2012).
- [31] M. Wu and X. C. Zeng, *Nano Lett.* **17**, 6309 (2017).
- [32] C. Huang, Y. Du, H. Wu, H. Xiang, K. Deng, and E. Kan, *Phys. Rev. Lett.* **120**, 147601 (2018).
- [33] W. Ding, J. Zhu, Z. Wang, Y. Gao, D. Xiao, Y. Gu, Z. Zhang, and W. Zhu, *Nat. Commun.* **8**, 14956 (2017).
- [34] R. W. Nunes and X. Gonze, *Phys. Rev. B* **63**, 155107 (2001).
- [35] M. Xu, C. Huang, Y. Li, S. Liu, X. Zhong, P. Jena, E. Kan, and Y. Wang, *Phys. Rev. Lett.* **124**, 067602 (2020).